


Article

Al₂O₃ Ceramic/Nanocellulose-Coated Non-Woven Separator for Lithium-Metal Batteries

Dong-Min Shin ^{1,2}, Hyunsu Son ^{1,†}, Ko Un Park ³, Junyoung Choi ¹, Jungdon Suk ^{1,4,*}, Eun Seck Kang ³, Dong-Won Kim ² and Do Youb Kim ^{1,*} 

¹ Energy Materials Research Center, Korea Research Institute of Chemical Technology, 141 Gajeong-ro, Yuseong-gu, Daejeon 34114, Republic of Korea

² Department of Chemical Engineering, Hanyang University, Seoul 04763, Republic of Korea

³ Advanced Materials Parts TP, Materials & Devices Advanced Research Center, Chief Technology Office, LG Electronics, W1, LG Science Park, 10, Magokjungang 10-ro, Gangseo-gu, Seoul 07796, Republic of Korea

⁴ Department of Chemical Convergence Materials, University of Science and Technology, 217 Gaejeong-ro, Yuseong-gu, Daejeon 34113, Republic of Korea

* Correspondence: jdsuk@kriect.re.kr (J.S.); dykim@kriect.re.kr (D.Y.K.)

† Current Address: Advanced Pouch Cell Development Team 2, Mobility & IT Battery Development, LG Energy Solution, 188, Munji-ro, Yuseong-gu, Daejeon 34122, Republic of Korea.

Abstract: Separators play an essential role in lithium (Li)-based secondary batteries by preventing direct contact between the two electrodes and providing conduction pathways for Li-ions in the battery cells. However, conventional polyolefin separators exhibit insufficient electrolyte wettability and thermal stability, and in particular, they are vulnerable to Li dendritic growth, which is a significant weakness in Li-metal batteries (LMBs). To improve the safety and electrochemical performance of LMBs, Al₂O₃ nanoparticles and nanocellulose (NC)-coated non-woven poly(vinylidene fluoride)/polyacrylonitrile separators were fabricated using a simple, water-based blade coating method. The Al₂O₃/NC-coated separator possessed a reasonably porous structure and a significant number of hydroxyl groups (-OH), which enhanced electrolyte uptake (394.8%) and ionic conductivity (1.493 mS/cm). The coated separator also exhibited reduced thermal shrinkage and alleviated uncontrollable Li dendritic growth compared with a bare separator. Consequently, Li-metal battery cells with a LiNi_{0.8}Co_{0.1}Mn_{0.1}O₂ cathode and an Al₂O₃/NC-coated separator using either liquid or solid polymer electrolytes exhibited improved rate capability, cycle stability, and safety compared with a cell with a bare separator. The present study demonstrates that combining appropriate materials in coatings on separator surfaces can enhance the safety and electrochemical performance of LMBs.

Keywords: nanocellulose; Al₂O₃; lithium-metal battery; safety; stability



Citation: Shin, D.-M.; Son, H.; Park, K.U.; Choi, J.; Suk, J.; Kang, E.S.; Kim, D.-W.; Kim, D.Y. Al₂O₃ Ceramic/Nanocellulose-Coated Non-Woven Separator for Lithium-Metal Batteries. *Coatings* **2023**, *13*, 916. <https://doi.org/10.3390/coatings13050916>

Academic Editor: Ning Sun

Received: 24 April 2023

Revised: 8 May 2023

Accepted: 11 May 2023

Published: 13 May 2023



Copyright: © 2023 by the authors. Licensee MDPI, Basel, Switzerland. This article is an open access article distributed under the terms and conditions of the Creative Commons Attribution (CC BY) license (<https://creativecommons.org/licenses/by/4.0/>).

1. Introduction

Lithium (Li)-ion batteries (LIBs) are regarded as excellent power sources for electronic devices, electric vehicles (EVs), and large-scale energy storage systems (ESSs) owing to their high energy density, good cycle performance, and small self-discharge capacity [1,2]. Typically, LIBs consist of four main components: the cathode, anode, separator, and electrolyte. Among them, the separator plays a decisive role in isolating the cathode and anode to prevent physical contact and providing channels for Li-ion travel inside the battery cell [3–5]. At present, microporous polyolefin separators, including polyethylene (PE) and polypropylene (PP), are widely used in LIBs owing to their good mechanical properties and excellent chemical stability. However, polyolefin separators have some fundamental limitations that must be resolved for general LIB applications [6–8]. Commonly, non-polar polyolefin separators exhibit relatively poor wetting with polar organic liquid electrolytes, which eventually leads to an increase in the internal resistance of LIBs [9–11]. Moreover, the relatively low melting temperature of commercial polyolefin separators (130 °C for PE

and 165 °C for PP) leads to shrinkage of the separators in a high-temperature environment, which can cause a fire or even an explosion owing to direct contact between the cathode and anode in a battery cell [11,12]. Hence, their insufficient electrolyte wettability and poor thermal stability render them unable to meet the needs of high-performance LIBs.

To overcome these drawbacks, a large number of researchers have contributed to the development of novel LIB separators. Among various approaches, the use of an inorganic ceramic particle coating on the separator surface has attracted considerable attention owing to its simple operating process, relatively easy thickness control of the separator, and low cost [13–15]. In addition, inorganic ceramic particles such as SiO₂, Al₂O₃, and TiO₂ can not only improve the absorption of the liquid electrolyte, but also enhance the thermal stability of the separators [6,7,16–18]. For example, Shi et al. fabricated Al₂O₃ powder-coated PE separators [6], and Zheng et al. reported SiO₂ nanoparticle-coated PE separators [18]. These coated separators showed improved thermal stability, good wettability, and higher uptake of liquid electrolyte than bare PE separators. In addition, LIB cells using the coated separators exhibited improved electrochemical performance compared with cells using bare PE separators.

An alternative material to enhance the properties of separators is nanocellulose (NC), which is a cellulosic material with one dimension in the nanometer range, and is considered a promising material owing to its high mechanical properties and outstanding electrolyte wettability [19,20]. In addition, cellulose is the most abundant natural polymeric material on earth, is renewable and biodegradable with thermal dimensional stability. Despite these benefits, the relatively high production cost of NC is a major drawback. However, cellulose shows a good affinity with polar liquid electrolytes owing to its many hydrophilic components, such as hydroxyl groups (-OH) and has good mechanical properties with abundant hydrogen bonds between the cellulose fibers [9,20,21]. Accordingly, researchers have attempted to fabricate functional separators using NC to enhance the safety and electrochemical performance of LIB cells [22–26]. However, most studies have focused on constructing porous separators using NC as the base material. Recently, Pan et al. reported that an NC-modified PE separator could stabilize Li-metal anodes by regulating the Li-ion flux and mitigating Li dendrite growth, eventually improving the cycle performance of LIB cells [20]. The results demonstrated that NC is an excellent coating material for high-performance separators; nevertheless, studies on NC-coated separators have rarely been reported.

We speculated that if an appropriate amount of NC were incorporated into the ceramic particle coating layer, it could enhance the electrolyte uptake without pore clogging. Accordingly, a simple, water-based and cost-effective blade coating method was applied to fabricate Al₂O₃/NC composite-coated poly(vinylidene fluoride)/polyacrylonitrile (PVdF/PAN) non-woven separators. To the best of our knowledge, this is the first report on separators coated with ceramic particles and NC. Introducing NC in a coating layer can improve the hydrophilicity of the separator surface and the wettability in electrolytes. In addition, NC acts as a spacer between the Al₂O₃ particles, which provides the coated separator with a more suitable pore structure for electrolyte penetration. Consequently, the coated separator showed higher electrolyte uptake, up to 394%, and enhanced ionic conductivity. The coated separator also exhibited improved thermal stability and mitigated Li dendrite growth. As a result, NCM811//liquid electrolyte (LE)//Li LIB cells using the Al₂O₃/NC-coated separator exhibited enhanced rating capability and cycle stability compared with cells using a bare PVdF/PAN separator. Furthermore, a solid polymer electrolyte (SPE) was also applied to the coated separators to fabricate Li polymer battery (LPB) cells. The coated separator also enhanced the electrochemical performance of the NCM811//SPE//Li LPB cells at room temperature.

2. Experimental Section

2.1. Materials

A poly(vinylidene fluoride)/polyacrylonitrile non-woven separator (PVdF/PAN, thickness = 30 μm) was purchased from Amgreentech Co. Ltd. and used as a base separator. Aqueous nanocellulose (NC) solution (1 wt%) was obtained from LG Electronics (Seoul, Republic of Korea). Aluminum oxide (Al_2O_3 , average particle size = 480 nm; AES-11, Sumitomo Chemical Co., Tokyo, Japan), sodium carboxymethyl cellulose (CMC, WS-C, Dai-ichi Kogyo Seiyaku Co., Ltd., Tokyo, Japan), disodium laureth sulfosuccinate (28 wt% ASCO[®] DLSS, AK Chemtech Co., Ltd., Seoul, Republic of Korea), poly(ethylene glycol) dimethyl ether (PEGDME, average Mw = 500, Sigma-Aldrich, St. Louis, MO, USA), and fluoroethylene carbonate (FEC, Sigma-Aldrich, 99%) were purchased and used as received. Bisphenol A ethoxylate diacrylate (BPh-A, average Mw = 688, Hannog Chemical, Gunsan, Republic of Korea) and *t*-butyl peroxyisobutyrate (Seki Arkema Co., Haman-gun, Republic of Korea) were used as received. Lithium bis(trifluoromethanesulfonyl) imide (LiTFSI, Sigma-Aldrich, 99.95%) was dried in a vacuum oven at 120 $^\circ\text{C}$ before use. In all experiments, deionized (DI) water with a resistivity of 18.2 M Ω , which was prepared using a Milli-Q ultrapure water system (Millipore, Burlington, VT, USA), was used.

2.2. Preparation of Al_2O_3 /NC-Coated Separators

Coating slurries with various Al_2O_3 and NC weight ratios were prepared by mixing aqueous stock solutions of Al_2O_3 (52 wt%) and NC (1 wt%) in various ratios. Aqueous solutions of 2 wt% CMC (as a binder) and 1 wt% DLSS (as a surfactant) were then added and mixed homogeneously. The coating slurries were then cast onto a bare PVdF/PAN separator using a doctor blade, and the coated separators were dried in a convection oven at 60 $^\circ\text{C}$ for 4 h. The Al_2O_3 /NC-coated separator is denoted by Al_2O_3 /NC-X, where X represents the mass ratio of NC (out of 10) in the Al_2O_3 /NC composite. Table S1 in the Supporting Information (SI) summarizes the weight of Al_2O_3 , the NC stock solutions for preparing coating solutions, and the resulting weight ratio between Al_2O_3 and NC.

2.3. Characterization

The surface morphologies of the samples were observed using a field-emission scanning electron microscope (FE-SEM, JSM-6700F, JEOL, Tokyo, Japan) at an accelerating voltage of 10 kV. The water contact angle was evaluated using a contact angle tester (SEO300A, Surface and Electrooptics Co., Suwon, Republic of Korea). The Gurley values for the samples were obtained using a Gurley densometer (Model 4110 N, Gurley Precision Instruments, Troy, MI, USA) by measuring the time required for 100 cc of air to pass through under a pressure of 0.02 MPa. The thermal shrinkage of the separators was calculated by measuring their dimensions before and after heating at different temperatures for 15 min according to the following equation:

$$\text{Thermal shrinkage} = (D - D_0)/D_0 \times 100\%, \quad (1)$$

where D_0 and D represent the areas of the separator before and after heating, respectively. The electrolyte uptake of the different separators was measured by immersing the separators in an electrolyte (1 M LiPF_6 in ethylene carbonate (EC)/diethyl carbonate (DEC) (1:1 v/v)). The electrolyte-soaked separators were weighed after removing redundant electrolyte using wipes. The electrolyte uptake can be calculated using Equation (2):

$$\text{Uptake} = (W - W_0)/W_0 \times 100\%, \quad (2)$$

where W and W_0 are the weights of the wet separator with the electrolyte and the dry separator, respectively.

2.4. Electrochemical Measurements

To evaluate the electrochemical performances of the samples, CR2032 coin-type cells were assembled in an Ar-filled glove box ($\text{H}_2\text{O} < 1$ ppm, MBraun, Velbert, Germany). The ionic conductivity was measured via electrochemical impedance spectroscopy (EIS) using a potentiostat with a built-in EIS (VMP3, Biologic, Seyssinet-Pariset, France) at room temperature. Cells for the EIS measurements were fabricated using two stainless steel (SUS) electrodes (0.125 mm thick, Hohsen Co., Osaka, Japan) with various separator samples. The scanning frequency ranged from 0.1 Hz to 65 kHz with a small perturbation voltage of 10 mV AC amplitude. The ionic conductivity was calculated using the following equation:

$$\sigma = d / (R_b \times S), \quad (3)$$

where σ , d , R_b , and S represent the ionic conductivity, thickness of the separator, bulk resistance, and electrode area, respectively. The electrochemical stability window was measured by linear sweep voltammetry (LSV) using a potentiostat (VMP3, Biologic) with a working electrode of SUS and a counter electrode of Li at a scan rate of 1.0 mV/s from open circuit voltage (OCV) to 6.0 V (vs. Li/Li⁺).

Li plating/stripping tests and LIB performance were evaluated using Li//Li symmetric cells and LiNi_{0.8}Co_{0.1}Mn_{0.1}O₂(NCM811)//Li half-cells, respectively, with a liquid electrolyte (LE, 1.0 M LiPF₆ in EC/DEC (1:1 v/v) with 5 wt% of FEC) as well as a solid polymer electrolyte (SPE). The NCM811 (POSCO Chem., Pohang, Republic of Korea) cathode was fabricated by casting a slurry containing NCM811 powder, Super P, and PVdF at a mass ratio of 65.5:1.5:2 in *N*-methyl-2-pyrrolidone (NMP) on an Al-foil current collector, which was then dried in an oven at 100 °C for 24 h. The loading of the NCM811 active material was fixed at ~7.0 mg/cm². To fabricate the SPE-loaded cells, an SPE precursor solution was prepared. The Li salt (LiTFSI) was mixed with a plasticizer, PEGDME, for 24 h. Then, BPh-A (as a crosslinking agent) and FEC (5 wt%, as an electrolyte additive) were added to the mixed solution. The ratio of PEGDME to BPh-A was fixed at 8:2 by weight, and the concentration of the Li salt was adjusted to obtain an [EO]/[Li⁺] molar ratio of 20. *t*-BPP at 1 wt% with respect to BPh-A was mixed with the precursor solution as an initiator before use. Test cells loaded with SPE were assembled with the SPE precursor solution-soaked separator, and the cells were then placed in an oven at 90 °C for 30 min for crosslinking [27,28]. The LIB test was performed in the voltage range of 3.0–4.2 V (vs. Li/Li⁺).

3. Results and Discussion

The Al₂O₃/NC composite-coated separators with various mass ratios of Al₂O₃ and NC (Al₂O₃/NC-*X*, where *X* represents the mass ratio of NC out of 10 of the Al₂O₃/NC composite) were fabricated by water-based coating slurries on a PVdF/PAN non-woven base separator using a doctor blade (see the Section 2 for details). Briefly, coating slurries were prepared by mixing Al₂O₃ particles, NC, sodium carboxymethyl cellulose (CMC) as a binder and disodium laureth sulfosuccinate (DLSS) as a surfactant in DI water. DLSS is an anionic surfactant and it is well-known that it is electrochemically stable up to 4.4 V vs. Li/Li⁺ [29]. It not only improves dispersion stability of the coating materials in a slurry but also enhances the wettability of coating slurry on a separator surface [29,30]. In our experiments also, DLSS played a key role in enhancing the quality of coating layer. As shown in Figure S1 in the SI, a coating layer without DLSS was not stable enough and easily detached from a base separator surface even during a brief time in water. On the contrary, a coating slurry with DLSS could produce a conformal and stable coating layer due to well-dispersed coating materials and enhanced wettability on the base separator surface.

Figure 1 shows the top-view scanning electron microscope (SEM) images of the bare PVdF/PAN and Al₂O₃/NC-*X* separators. As shown in Figure 1a, a bare PVdF/PAN separator consists of numerous nanofibers with diameters of approximately 200–500 nm and a large number of voids between individual nanofibers. The surfaces of the coated

separators were completely covered with coating materials (e.g., Al_2O_3 and NC). Figure 1b shows the SEM image of a separator coated with only Al_2O_3 ($\text{Al}_2\text{O}_3/\text{NC}-0$), where the base separator was concealed by an Al_2O_3 coating layer with pores smaller than those of the base separator. When the mass ratio of NC was relatively low (not greater than three), there were no obvious changes in the surface morphology compared with $\text{Al}_2\text{O}_3/\text{NC}-0$, even though NC was visible (Figure S2a in the SI and Figure 1c). The red arrows in Figure 1c indicate NC particles between the Al_2O_3 particles. As the NC mass ratio increased, a larger number of NC particles were observed on the surface of the coated separators, and the pores between the Al_2O_3 particles were blocked (Figure S2b in the SI and Figure 1d). A further increase in the mass ratio of NC eventually clogged most of the pores (Figure S2c in the SI), thereby hindering the migration of Li ions through the separator. The thickness of the coating layer was approximately $5\ \mu\text{m}$ for all the coated separators (Figure S3 in the SI). XRD patterns obtained from the coated separators exhibited sharp peaks for $\alpha\text{-Al}_2\text{O}_3$, and broad peaks for PAN and PVdF (Figure S4 in the SI). However, since the amount of NC was relatively small and had a relatively lower degree of crystallinity than the Al_2O_3 particles, peaks for NC were not observed. Figure S5 in the SI shows energy dispersive X-ray spectroscopy mapping images of coated separators.

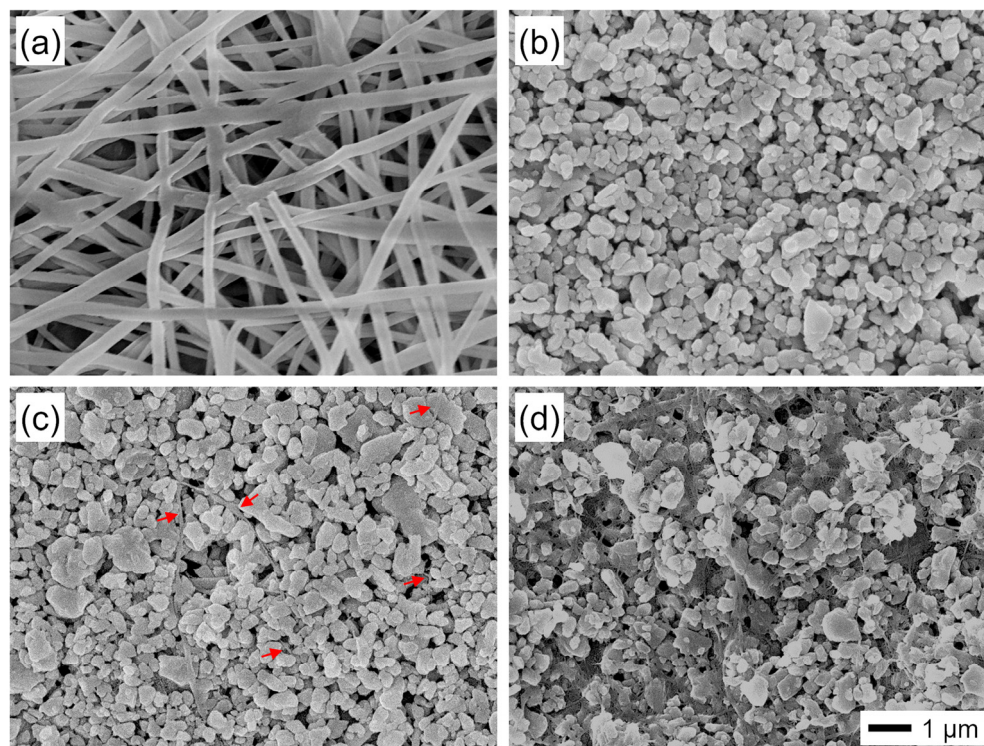


Figure 1. Top-view scanning electron microscope (SEM) images of (a) bare PVdF/PAN, (b) $\text{Al}_2\text{O}_3/\text{NC}-0$, (c) $\text{Al}_2\text{O}_3/\text{NC}-3$, and (d) $\text{Al}_2\text{O}_3/\text{NC}-7$ separators. Red arrows in (c) indicate NCs. All images have an identical magnification.

The wetting behavior is an important property of separators. Figure 2a shows the contact angles of deionized water on the separator samples. The bare PVdF/PAN separator exhibited a relatively high contact angle of 85° because of the hydrophobic nature of the bare PVdF/PAN separator surface. When the base separator was coated with Al_2O_3 , the contact angle decreased substantially owing to the hydrophilic character of the Al_2O_3 particles, even though it still exhibited a contact angle of 20° . In contrast, the $\text{Al}_2\text{O}_3/\text{NC}-3$ and $\text{Al}_2\text{O}_3/\text{NC}-7$ separators were completely wet with deionized water and exhibited an astonishingly low contact angle of 0° . This could be attributed to the addition of NC with abundant hydrophilic polar $-\text{OH}$ groups on its surface. A small contact angle tends to result in better wettability of the electrolyte, which can affect the electrolyte uptake,

ionic conductivity of the separator, and eventually, the electrochemical performance of the battery [25,31]. The electrolyte wetting behavior of the separator samples was also evaluated using several electrolytes with various polarity indices (Figure S6 in the SI). All the separator samples, including the base separator, exhibited good wettability to the electrolyte solvents.

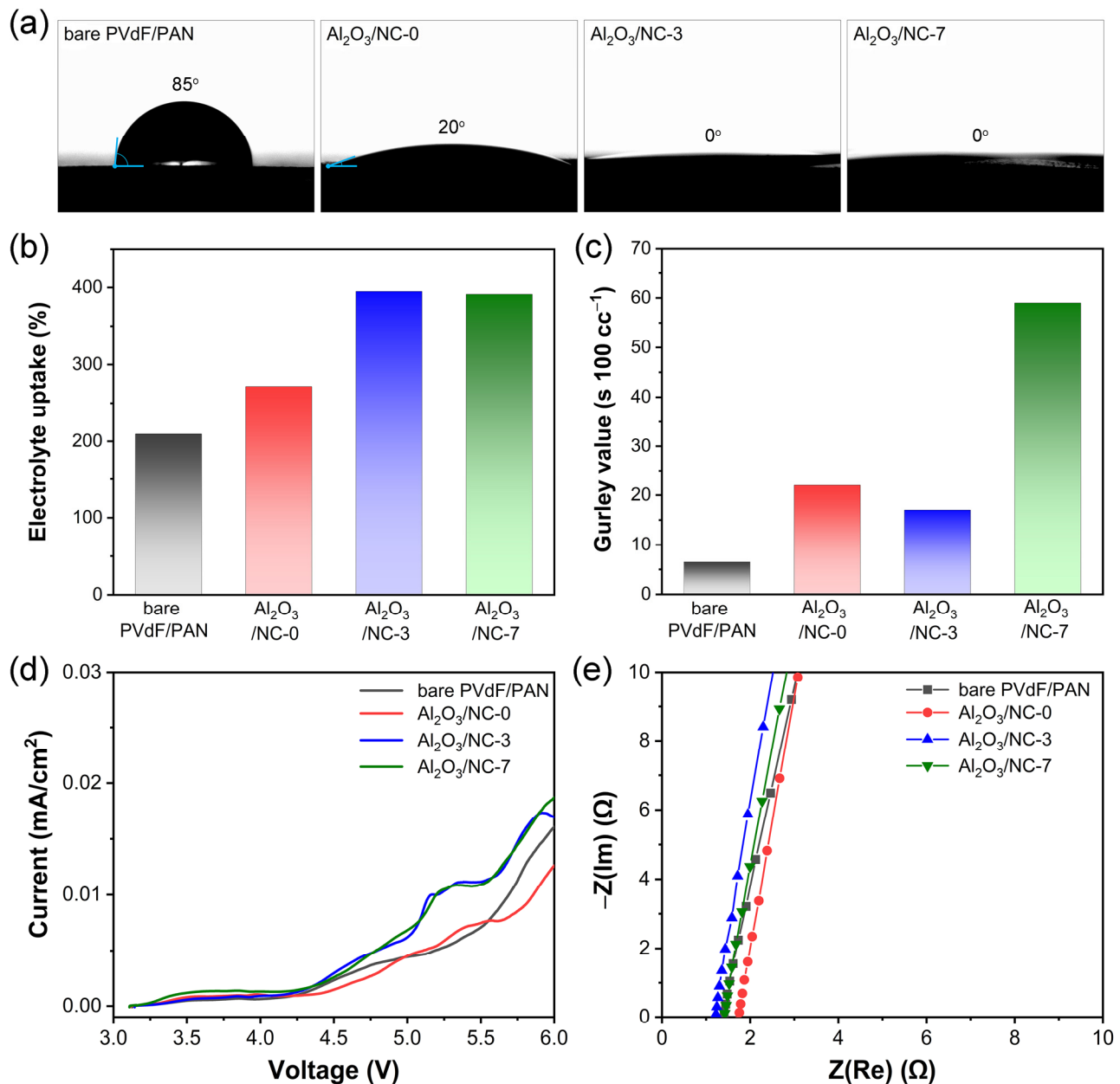


Figure 2. (a) Water contact angles on the separator samples, (b) electrolyte uptake, and (c) Gurley value of the separator samples. (d) Linear sweep voltammetry curves of SUS//Li cells and (e) Nyquist plots of SUS//SUS cells using the separator samples.

The electrolyte uptake of the separators, which represents the ability of a separator to retain an electrolyte solution, was also evaluated (Figure 2b). The electrolyte uptake of the bare PVdF/PAN was 209.5% and that of the Al₂O₃/NC-0 was 271.6%. The superior wetting ability of the separators coated with Al₂O₃ and NC enabled enhanced electrolyte uptake of 394.8% and 391.2% for Al₂O₃/NC-3 and Al₂O₃/NC-7, respectively.

The air permeability of the separator samples was determined by the Gurley method, which measures the time required for 100 cc of air to pass through the separator samples

(Figure 2c and Figure S7 in the SI). The bare PVdF/PAN had a large number of submicron pores and thus showed a relatively low Gurley value of 6.5 s. Al₂O₃/NC-0 exhibited an increased Gurley value of 22 s because the bare PVdF/PAN surface was covered with Al₂O₃ particles. However, when a small amount of NC was added to the coating layer, the Gurley values of the separators were slightly decreased; the values for Al₂O₃/NC-1 and Al₂O₃/NC-3 were 18 s and 17 s, respectively. This can be explained by the small amount of NC acting as a spacer, and the close packing of the Al₂O₃ particles was interrupted by the NC. The reduced amount of Al₂O₃ in the coating layer could be one of the reasons for the decreased Gurley values of the samples. As the NC mass ratio was further increased, the Gurley values of the separator samples rebounded because a relatively large amount of NC blocked the pores of the coating layers. Al₂O₃/NC-5, Al₂O₃/NC-7, and Al₂O₃/NC-9 exhibited Gurley values of 19 s, 59 s, and 231 s, respectively.

Figure 2d shows the linear sweep voltammetry (LSV) curves of the SUS//Li cells using the separator samples. Although the curves gradually increased from approximately 4.3 V, the current was relatively low and resembled that of the bare PVdF/PAN separator. This result implies that the electrochemical stability of the coated separators is comparable with that of the bare PVdF/PAN separator and is suitable for battery applications. Figure 2e shows Nyquist plots of the SUS/SUS cells obtained using the separator samples. The ionic conductivities of the separator samples were determined using the bulk resistances indicated by the high-frequency x-axis intercepts. The ionic conductivity of bare PVdF/PAN was 1.07 mS/cm and that of Al₂O₃/NC-0 was 1.04 mS/cm. However, the Al₂O₃/NC-3 and Al₂O₃/NC-7 separators exhibited enhanced ionic conductivities of 1.49 and 1.28 mS/cm, respectively. These values were approximately 40% and 20% higher than those for of the bare PVdF/PAN separator. Generally, the ionic conductivity of a separator is related to its electrolyte uptake ability and pore structure, which provides channels for the transportation of ions [31–33]. Therefore, the superior ionic conductivity of Al₂O₃/NC-3 was attributed to a relatively low Gurley value (17 s) and high electrolyte uptake (394.8%). The higher ionic conductivity of the Al₂O₃/NC-3 separator not only improved the discharge capacity but also promoted the transport of lithium ions [34,35]. Table 1 summarizes the properties of the separator samples.

Table 1. Comparison of properties of a bare PVdF/PAN and Al₂O₃/NC-X-coated separators.

Sample	Thickness (μm)	Electrolyte Uptake (%)	Gurley Number (s)	Ionic Conductivity (mS/cm)
bare PVdF/PAN	30	209.5	6.5	1.07
Al ₂ O ₃ @NC-0	35	271.6	22	1.04
Al ₂ O ₃ @NC-3	35	394.8	17	1.49
Al ₂ O ₃ @NC-7	35	391.2	59	1.28

The excellent thermal stability of separators is essential for battery safety as it can avoid explosions caused by short circuits at elevated temperatures. To verify the thermal stability of the separator samples, their morphological changes and shrinkage were examined after treatment at a series of temperatures for 15 min (Figure 3). The differences in the dimensional stability of the separator samples after treatment at elevated temperatures were obvious (Figure 3a). The shrinkage of the separator samples was quantified using the normalized cross-sectional area (Figure 3b). In the case of the bare PVdF/PAN separator, a 4% thermal shrinkage was observed at a relatively low temperature of 100 °C. It further shrank as temperature increased and maintained only 46% of its original size after being treated at 250 °C. Meanwhile, owing to the excellent thermal stability of the Al₂O₃ particles and NC, all the Al₂O₃/NC-X samples displayed significantly improved thermal durability compared with the bare PVdF/PAN separator. The Al₂O₃/NC-0 separator exhibited the best thermal stability; it maintained 95% of its original size after being treated at 250 °C. Because the thermal stability of NC is inferior to that of Al₂O₃, the thermal shrinkage of Al₂O₃/NC-X increased as the mass ratio of NC increased. After being heated at 150 °C,

$\text{Al}_2\text{O}_3/\text{NC}$ -3 and $\text{Al}_2\text{O}_3/\text{NC}$ -7 maintained 100% and 95% of their original sizes, respectively. Even after being heated at 250 °C, $\text{Al}_2\text{O}_3/\text{NC}$ -3 and $\text{Al}_2\text{O}_3/\text{NC}$ -7 still retained 79% and 72% of their original sizes, respectively. These values are far higher than those of the bare PVdF/PAN separator (46%). The morphological changes and shrinkages of all the separator samples after treatment at elevated temperatures are shown in Figures S8 and S9 in the SI, respectively. The results show that the $\text{Al}_2\text{O}_3/\text{NC}$ coating layer significantly enhanced the thermal stability and effectively reduced the thermal shrinkage of the separators, which could improve the safety of LIBs using coated separators.

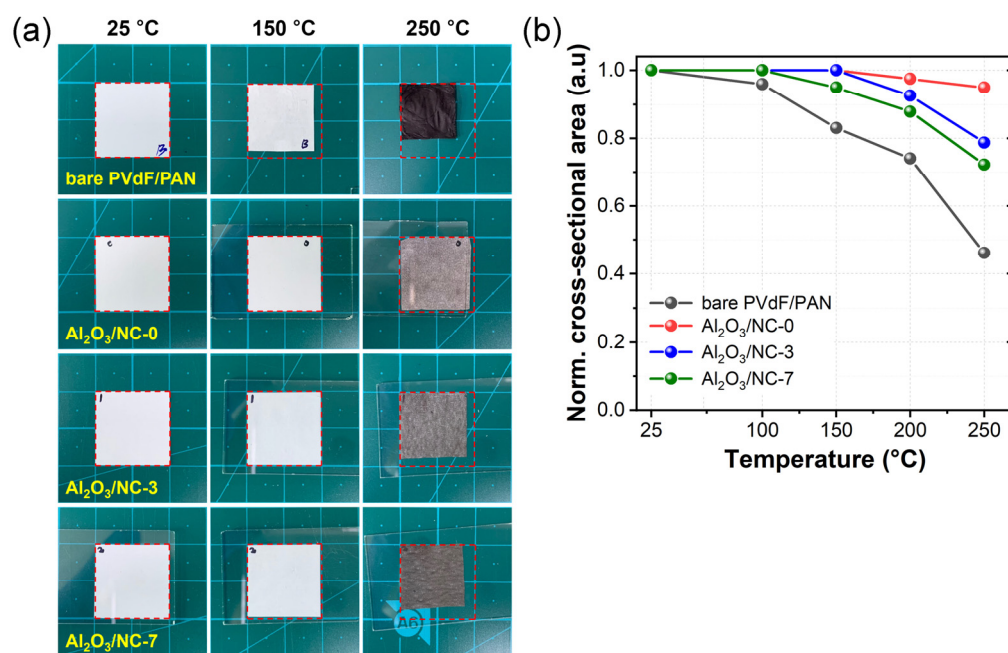


Figure 3. (a) Photographs showing thermal shrinkage of a bare PVdF/PAN and $\text{Al}_2\text{O}_3/\text{NC}$ -X-coated separators at ambient and elevated temperatures. (b) Comparison of normalized cross-sectional area of separator samples at various temperatures.

To investigate the cyclic stability of the separators, Li plating/stripping tests were performed using Li//LE//Li symmetric cells with different separators. Figure 4a shows the voltage profiles of the cells with a capacity of 1.0 mAh/cm² at a current density of 1.0 mA/cm². In a cell using a bare PVdF/PAN separator, the profile exhibited a gradual increase in the voltage hysteresis and a sudden drop at approximately 160 h. This phenomenon could be attributed to an internal short circuit in the cell owing to the non-homogeneous Li-ion flux and continuous growth of sharp Li dendrites on the surface of the Li electrode during the test [35,36]. In contrast, the cells using the coated separators showed more stable voltage responses with lower overpotentials and longer cycle lives than the cell using a bare PVdF/PAN separator. The cells using $\text{Al}_2\text{O}_3/\text{NC}$ -0, $\text{Al}_2\text{O}_3/\text{NC}$ -3, and $\text{Al}_2\text{O}_3/\text{NC}$ -7 separators also exhibited a gradual increase in the voltage hysteresis and short-circuited at approximately 240 h, 280 h, and 240 h, respectively. The improved cycle stability of the cells using the coated separators could be attributed to the enhanced electrolyte uptake and the coating layer could alleviate the growth of Li dendrites by regulating the Li-ion flux. For better comparison, Figure S10 in the SI shows the enlarged voltage profiles of these cells. Although the overpotentials gradually increased as the test progressed in all cells, cells using the coated separators displayed much lower overpotentials than that of the cell using a bare PVdF/PAN separator. Notably, the cell using the $\text{Al}_2\text{O}_3/\text{NC}$ -3 separator exhibited the lowest overpotential and longest cycle life among the samples. The superior electrolyte uptake and high ionic conductivity of the $\text{Al}_2\text{O}_3/\text{NC}$ -3 separator could facilitate the efficient movement of Li-ions in the cell and contribute to mitigating electrochemical polarization during cycling.

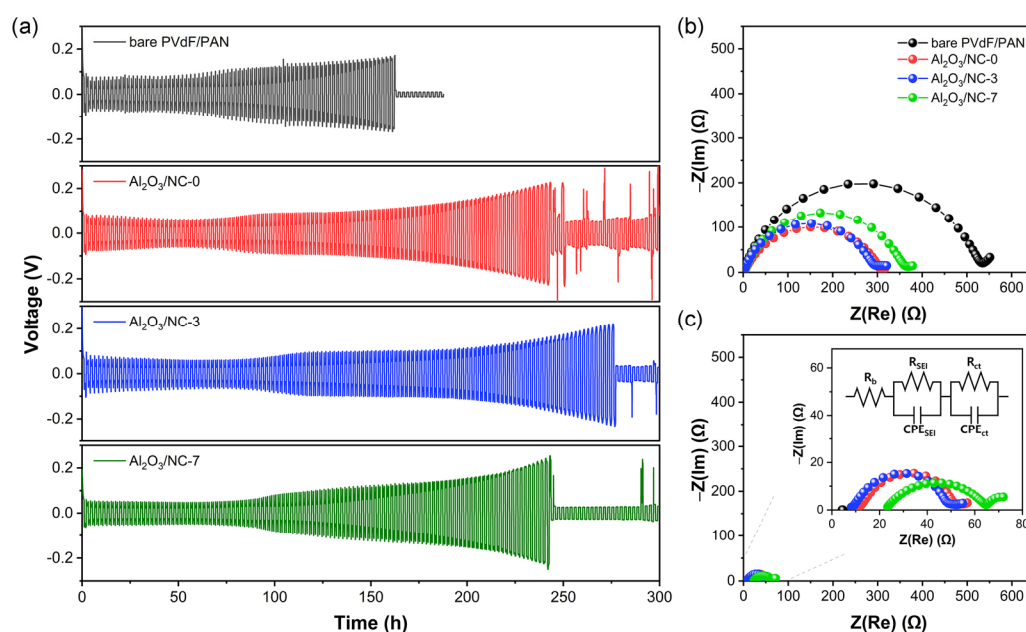


Figure 4. (a) Voltage profiles of Li plating/stripping in Li/LE/Li symmetric cells using different separators with a capacity of 1.0 mAh/cm² at a current density of 1.0 mA/cm². Nyquist plots of the symmetric cells using different separators (b) before and (c) after 100th plating/stripping cycle.

Figure 4b,c show the Nyquist plots of the cells using different separators before and after the 100th Li plating/stripping cycle, respectively. Generally, R_b in the high-frequency region of the alternating current (AC) impedance spectrum represents the bulk resistance, and the interfacial resistance of the middle- and low-frequency regions in the semi-cycle includes the solid electrolyte interface resistance (R_{SEI}) and charge transfer resistance (R_{ct}) [33,36,37]. According to the fitted results, the interfacial resistance of the bare PVdF/PAN, Al₂O₃/NC-0, Al₂O₃/NC-3, and Al₂O₃/NC-7 separators before cycling was 537.4, 306.8, 301.5 and 369.9 Ω, respectively. The Al₂O₃/NC-3 separator showed the lowest interfacial resistance compared with the other separators, which can be attributed to the superior properties of the Al₂O₃/NC-3 separator, such as better affinity with a liquid electrolyte and high electrolyte uptake [7,14,38,39]. Furthermore, the cell using the Al₂O₃/NC-3 separator retained a lower resistance after 100 cycles (Figure 4c); this is consistent with the lowest overpotentials at the 100th cycle in the voltage profiles of the Li plating/stripping test (Figure 4a and Figure S10 in the SI). These results suggest that the Al₂O₃/NC-3 separator possesses better interfacial compatibility with the electrolyte and lithium electrode, which, in turn, affects the high C-rate and stable cycle performance of the battery cell.

In addition, a functional separator with a higher mechanical strength can alleviate Li dendrite growth [40,41]. The growth of Li dendrite can cause a rapid decline in cell performance due to the continuous decomposition of an electrolyte and the formation of a thick SEI layer on the Li anode [42,43]. Additionally, it can lead to cell explosion due to short-circuiting. Therefore, investigating the morphological changes in Li is crucial in the development of Li metal-based batteries [44–50]. To verify the ability of the coated separator to suppress the dendritic growth of Li, the morphology of Li was examined after Li plating/stripping cycles using SEM. Figure 5a,b show the top-view SEM images of Li after the 10th Li plating/stripping cycle in Li/LE/Li symmetric cells using bare PVdF/PAN and Al₂O₃/NC-3 separators, respectively. In the cell using the bare PVdF/PAN separator, Li deposits were composed of numerous Li dendrites and masses, rendering a rough and porous morphology (Figure 5a). By contrast, Li deposits in the cell using the Al₂O₃/NC-3 separator showed a relatively dense and smooth surface. These SEM results prove that the Al₂O₃/NC coating layer uniformly distributed the Li ions through the pores of the coating

layer and also inhibited the extensive growth of Li dendrites owing to its relatively high mechanical strength [51–53].

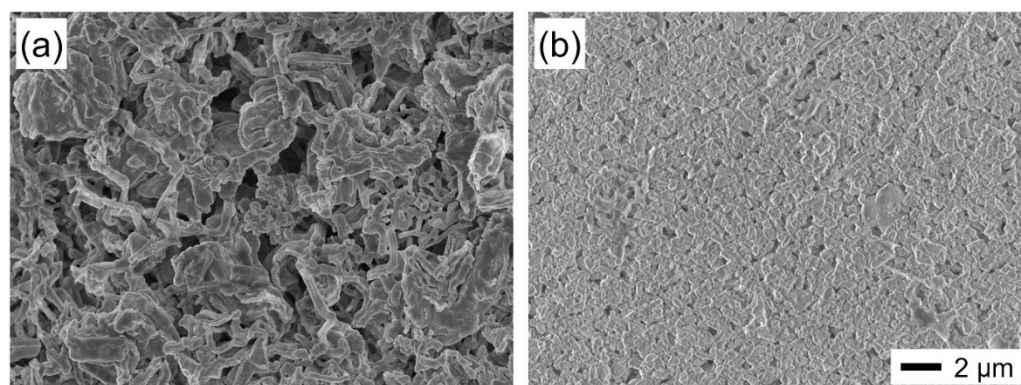


Figure 5. Top-view SEM images of lithium anodes in Li/LE/Li symmetric cells using (a) bare PVdF/PAN and (b) $\text{Al}_2\text{O}_3\text{@NC-3}$ separators after 10 plating/stripping cycles with a capacity of 1.0 mAh/cm^2 at a current density of 1.0 mA/cm^2 . The images have an identical magnification.

Encouraged by these results, NCM811//LE//Li cells using different separators were assembled to investigate the effect of the coating layer on the electrochemical performance of the LIB cells. As shown in Figure 6a, all the cells displayed similar voltage profiles and specific capacities during the 1st cycle at a current density of 0.1 C-rate. Discharge capacities of 199.6, 194.1, 198.2, and 195.1 mAh/g were noted for the cells using the bare PVdF/PAN, $\text{Al}_2\text{O}_3\text{/NC-0}$, $\text{Al}_2\text{O}_3\text{/NC-3}$, and $\text{Al}_2\text{O}_3\text{/NC-7}$ separator, respectively. When the current density was gradually increased to 2.0 C-rate, the cell using the $\text{Al}_2\text{O}_3\text{/NC-3}$ separator displayed the best rate capability among all the cells. The cell using the $\text{Al}_2\text{O}_3\text{/NC-3}$ separator delivered a discharge capacity of 146.4 mAh/g at 2.0 C-rate, which was higher than those for the cells using the bare PVdF/PAN (138.1 mAh/g), $\text{Al}_2\text{O}_3\text{/NC-0}$ (140.6 mAh/g), and $\text{Al}_2\text{O}_3\text{/NC-7}$ (121.1 mAh/g) (Figure 6b and Figure S11 in the SI). The higher rate capability of the cell using $\text{Al}_2\text{O}_3\text{/NC-3}$ can be attributed to the improved electrolyte uptake and ionic conductivity of the separator, owing to the Al_2O_3 and NC coating layers.

Figure 6c shows the cycle performance of the cells using different separators at 0.5 C-rate. Based on these results, the highest capacity retention was achieved by the cell using the $\text{Al}_2\text{O}_3\text{/NC-3}$ separator (65.9%) after 120 charge/discharge cycles, as compared with the cells using the bare PVdF/PAN (57.1%), $\text{Al}_2\text{O}_3\text{/NC-0}$ (61.5%), and $\text{Al}_2\text{O}_3\text{/NC-7}$ (42.8%). Furthermore, electrochemical impedance spectroscopy (EIS) was performed on the cells using the bare PVdF/PAN and $\text{Al}_2\text{O}_3\text{/NC-3}$ separators; it was found that the cell using the $\text{Al}_2\text{O}_3\text{/NC-3}$ separator exhibited a lower resistance after the 1st and 100th cycles (Figure S12 in the SI). The lower resistance of the cell was beneficial for reducing the electrochemical polarization of the cell [54], which could contribute toward the improved cycle stability of the cell using the $\text{Al}_2\text{O}_3\text{/NC-3}$ separator. In addition, its ability to suppress Li dendrite growth and stabilize the Li deposit of the $\text{Al}_2\text{O}_3\text{/NC-3}$ separator, as shown in Figure 5, could also be a reason for the improved cycle stability of the cell.

To further confirm the thermal safety of the cells, the open-circuit voltages (OCVs) of the cells were monitored using bare PVdF/PAN and $\text{Al}_2\text{O}_3\text{/NC-3}$ separators before and after heat treatment at 120°C . As shown in Figure S13 of the SI, the OCV of the cell using a bare PVdF/PAN separator decreased abruptly after heating at 120°C ; this was likely caused by a short circuit induced by the thermal shrinkage of the separator. By contrast, the cell using the $\text{Al}_2\text{O}_3\text{/NC-3}$ separator maintained its OCV at approximately 3.4 V (vs. Li/Li^+), even after being heated at 120°C , without an abrupt decrease in the OCV.

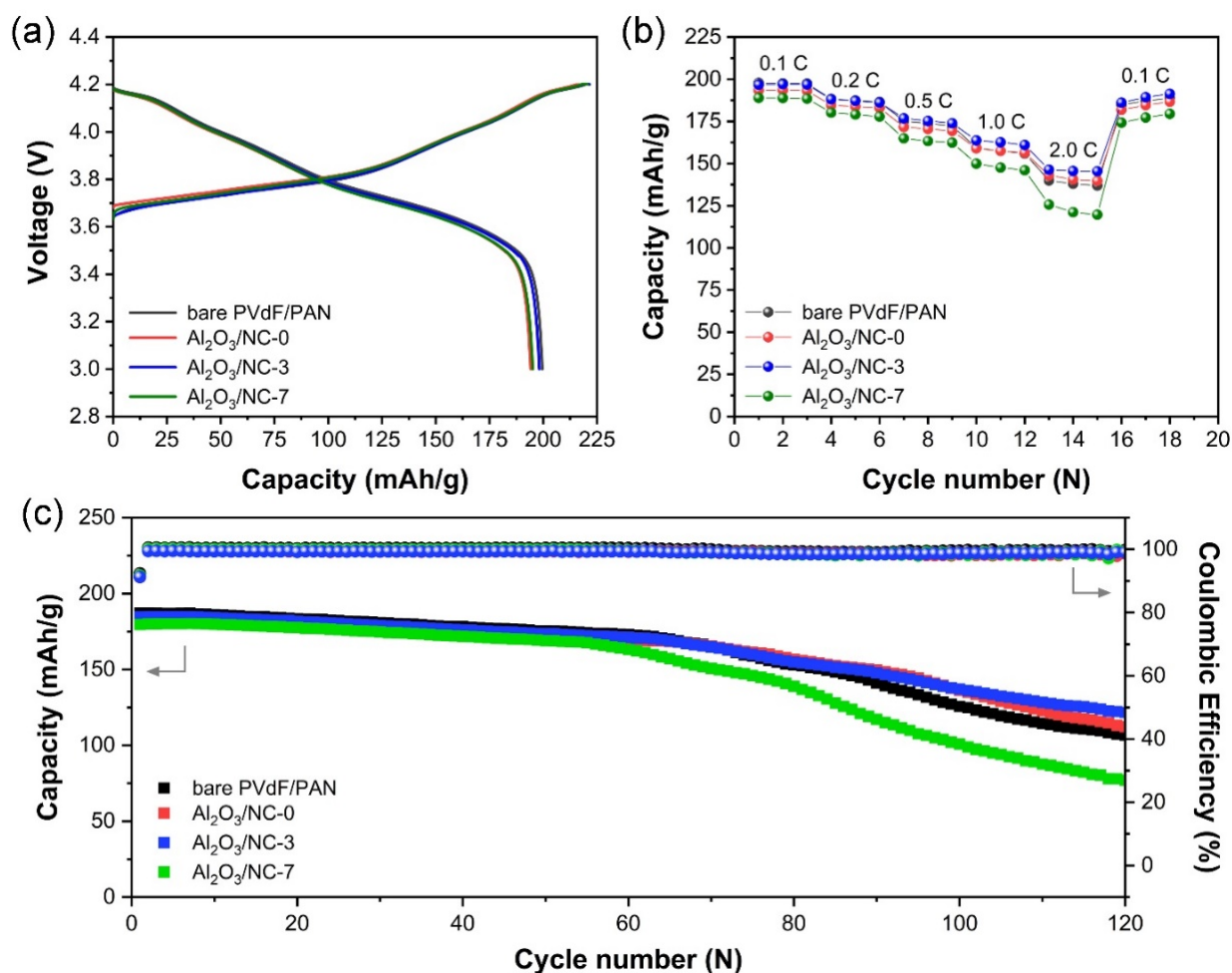


Figure 6. Electrochemical performance of NCM811/LE/Li half-cells using different separators; (a) voltage profiles at 0.1 C-rate, (b) C-rate performance, and (c) cycle stability at 0.5 C-rate.

Furthermore, we evaluated the applicability of the coated separators to LPBs by adopting an SPE. Figure S14 of the SI presents the voltage profiles during the Li plating/stripping test for the Li//SPE//Li symmetric cells using different separators at room temperature. As the ionic conductivity of the SPE used in this study was lower than that of the LE [27], the voltage profiles displayed higher overpotentials compared with those for the LE cases, even at lower current densities. Among these, the cell using Al₂O₃/NC-3 showed the best performance, with a stable voltage profile and the lowest overpotential across the experimental period. This result indicates that the Li ions could be sufficiently transferred through the SPE system within the separators. This result also implies that the porous structure of the Al₂O₃/NC-3 separator could induce a uniform Li distribution across the lithium electrode [52,55].

Moreover, NCM811//SPE//Li LPB cells with different separators were assembled, and their electrochemical performance was evaluated at room temperature. The cells exhibited inherently inferior electrochemical performances than the cells using LE, owing to the lower ionic conductivity of the SPE. However, the cells using Al₂O₃/NC-3 showed electrochemical performances equal to or greater than those of the other cells (Figure 7a,b and Figure S15 in the SI). Especially for the cycling test at 0.2 C-rate, the cell using Al₂O₃/NC-3 exhibited the highest discharge capacity of 123.5 mAh/g and a capacity retention of 77.8% at the 100th cycle. These values exceeded those for the cells using the bare PVdF/PAN (98.0 mAh/g, 65.1%), Al₂O₃/NC-0 (107.6 mAh/g, 73.4%), and Al₂O₃/NC-7 (52.0 mAh/g, 34.1%). These results also indicate that coated separators can be applied to LPBs to enhance their electrochemical performance. Finally, the electrochemical performance of our

LMB cells was compared with those of previously reported cells using a NCM811 cathode (Table S2 in the SI).

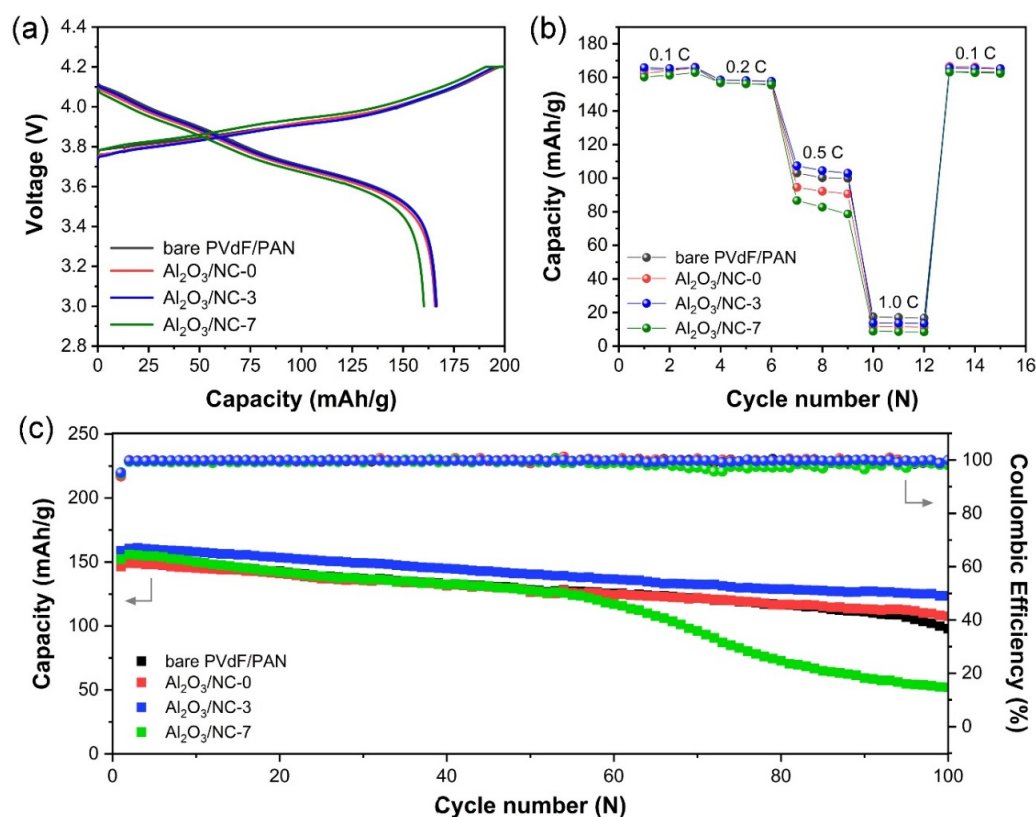


Figure 7. Electrochemical performance of NCM811/SPE/Li half-cells using different separators: (a) voltage profiles at 0.1 C-rate, (b) C-rate performance, and (c) cycle stability at 0.2 C-rate.

4. Conclusions

In summary, Al₂O₃/NC-coated PVdF/PAN separators were prepared for the first time by a simple aqueous blade coating method. The effects of the weight ratio between Al₂O₃ and NC in the coating layer on thermal stability and electrochemical performance of the separators were systematically investigated. Thanks to the inclusion of hydrophilic NC in the coating layer, the optimized Al₂O₃/NC-3-coated separator exhibited a good porous structure on the surface as well as improved electrolyte wettability, electrolyte uptake, and ionic conductivity. The separator also showed improved thermal durability with reduced thermal shrinkage at elevated temperatures in comparison to a bare separator. In addition, it was found that when the Al₂O₃/NC-3-coated separator was used, uncontrollable Li dendrite growth could be effectively alleviated by delocalized Li-ions and mechanical suppression. As a consequence, NCM811//LE//Li LIB cells using the Al₂O₃/NC-3 separator showed enhanced rate capability and superior cyclic performance than a cell using a bare separator. Furthermore, an SPE was also applied to the coated separators to evaluate their electrochemical performance in LPB cells. At room temperature, the NCM811//SPE//Li cell using the Al₂O₃/NC-3 separator also exhibited improved electrochemical performance compared with the cell with a bare separator. These findings suggest that combination of appropriate materials in the coating on a separator surface can enhance the safety and electrochemical performance of LMBs. Overall, Al₂O₃/NC-coated separators have the potential to provide large-scale Li-based secondary batteries with higher safety and electrochemical performance for application in EVs and ESS.

Supplementary Materials: The following supporting information can be downloaded at: <https://www.mdpi.com/article/10.3390/coatings13050916/s1>. Table S1: Weight of Al₂O₃ and NC stock solutions for preparing coating solutions and resulting weight ratio between Al₂O₃ and NC, Figure S1: Photographs of Al₂O₃/NC coated separators using coating slurries with or without DLSS, Figure S2: Top-view SEM images of (a) Al₂O₃/NC-1, (b) Al₂O₃/NC-5, and (c) Al₂O₃/NC-9 coated separators, Figure S3: (left) Cross-sectional SEM image of a Al₂O₃/NC-3 coated separator, and (right) photograph images showing separator samples and their thicknesses, Figure S4: XRD patterns of Al₂O₃/NC-0 and Al₂O₃/NC-3 separators, Figure S5: SEM-EDS mapping images of C, O, and Al for Al₂O₃/NC-0, Al₂O₃/NC-3, and Al₂O₃/NC-7 separators, Figure S6: Photographs showing wetting behavior of various solvents on different separators, Figure S7: Gurley value of the separator samples, Figure S8: Photographs showing thermal shrinkage of bare PVdF/PAN and Al₂O₃/NC coated separators at ambient and elevated temperatures, Figure S9: Comparison of normalized cross-sectional area of all separator samples, Figure S10: Enlarged voltage profiles of Li plating/stripping in Li/LE/Li symmetric cells using different separators with a capacity of 1.0 mAh/cm² at a current density of 1.0 mA/cm² shown in Figure 4, Figure S11: Charge-discharge voltage profiles of NCM811/LE/Li cells using different separators; (a) bare PVdF/PAN, (b) Al₂O₃@NC-0, (c) Al₂O₃@NC-3 and (d) Al₂O₃@NC-7 separators, Figure S12: Nyquist plots of NCM811/LE/Li half cells using bare PVdF/PAN and Al₂O₃/NC-3 coated separators (a) after 1 cycle and (b) 100 cycles at 0.5 C-rate, Figure S13: Plot of open circuit voltages of the NCM811/LE/Li cells using a bare PVdF/PAN and Al₂O₃/NC-3 separators at room temperature before and after heating at 120 °C, Figure S14: Voltage profiles of Li plating/stripping in Li/SPE/Li symmetric cells using different separators with a capacity of 0.4 mAh/cm² at a current density of 0.4 mA/cm², Figure S15: Charge-discharge voltage profiles of NCM811/SPE/Li cells using different separators; (a) bare PVdF/PAN, (b) Al₂O₃@NC-0, (c) Al₂O₃@NC-3 and (d) Al₂O₃@NC-7 separators, Table S2: Comparison of electrochemical performance of LMB cells using NCM811 cathode [56–69].

Author Contributions: Conceptualization, D.-M.S. and D.Y.K.; methodology, D.-M.S., H.S., K.U.P. and J.C.; validation, E.S.K., D.-W.K. and J.S.; formal analysis, D.-M.S. and K.U.P.; investigation, D.-M.S. and D.Y.K.; data curation, D.-M.S.; writing—original draft preparation, D.-M.S.; writing—review and editing, D.Y.K.; supervision, D.Y.K.; project administration, E.S.K. and J.S.; funding acquisition, E.S.K. and J.S. All authors have read and agreed to the published version of the manuscript.

Funding: This research was supported by Nano-Material Technology Development Program through the National Research Foundation of Korea (NRF) funded by Ministry of Science and ICT (NRF-2020M3H4A3081876 and NRF-2020M3H4A3082530).

Institutional Review Board Statement: Not applicable.

Informed Consent Statement: Not applicable.

Data Availability Statement: The data presented in this study are available on request from the corresponding author.

Conflicts of Interest: The authors declare no conflict of interest.

References

1. Kim, T.; Song, W.; Son, D.Y.; Ono, L.K.; Zi, Y. Lithium-ion batteries: Outlook on present, future, and hybridized technologies. *J. Mater. Chem. A* **2019**, *7*, 2942–2964. [[CrossRef](#)]
2. Zubi, G.; Dufo-López, R.; Carvalho, M.; Pasaoglu, G. The lithium-ion battery: State of the art and future perspectives. *Renew. Sustain. Energy Rev.* **2018**, *89*, 292–308. [[CrossRef](#)]
3. Yuan, B.; Wen, K.; Chen, D.; Liu, Y.; Dong, Y.; Feng, C.; Han, Y.; Han, J.; Zhang, Y.; Xia, C.; et al. Composite Separators for Robust High Rate Lithium Ion Batteries. *Adv. Func. Mater.* **2021**, *31*, 2101420. [[CrossRef](#)]
4. Lu, W.; Yuan, Z.; Zhao, Y.; Zhang, H.; Zhang, H.; Li, X. Porous membranes in secondary battery technologies. *Chem. Soc. Rev.* **2017**, *46*, 2199–2236. [[CrossRef](#)]
5. Xiang, Y.; Li, J.; Lei, J.; Liu, D.; Xie, Z.; Qu, D.; Li, K.; Deng, T.; Tang, H. Advanced Separators for Lithium-Ion and Lithium-Sulfur batteries: A Review of Recent Progress. *ChemSusChem* **2016**, *9*, 3023–3039. [[CrossRef](#)] [[PubMed](#)]
6. Shi, C.; Zhang, P.; Chen, L.; Yang, P.; Zhao, J. Effect of a thin ceramic-coating layer on thermal and electrochemical properties of polyethylene separator for lithium-ion batteries. *J. Power Sources* **2014**, *270*, 547–553. [[CrossRef](#)]
7. Yang, P.; Zhang, P.; Shi, C.; Chen, L.; Dai, J.; Zhao, J. The functional separator coated with core-shell structured silica-poly(methyl methacrylate) sub-microspheres for lithium-ion batteries. *J. Membr. Sci.* **2015**, *474*, 148–155. [[CrossRef](#)]

8. Shi, J.L.; Fang, L.F.; Li, H.; Zhang, H.; Zhu, B.K.; Zhu, L.P. Improved thermal and electrochemical performances of PMMA modified PE separator skeleton prepared via dopamine-initiated ATRP for lithium ion batteries. *J. Membr. Sci.* **2013**, *437*, 160–168. [[CrossRef](#)]
9. Zhu, C.; Zhang, J.; Xu, J.; Yin, X.; Wu, J.; Chen, S.; Zhu, Z.; Wang, L.; Wang, H. Facile fabrication of cellulose/polyphenylene sulfide composite separator for lithium-ion batteries. *Carbohydr. Polym.* **2020**, *248*, 116753. [[CrossRef](#)]
10. Kim, K.J.; Kwon, Y.K.; Yim, T.; Choi, W. Functional separator with lower resistance toward lithium ion transport for enhancing the electrochemical performance of lithium ion batteries. *J. Ind. Eng. Chem.* **2019**, *71*, 228–233. [[CrossRef](#)]
11. Sun, G.; Guo, J.; Niu, H.; Chen, N.; Zhang, M.; Tian, G.; Qi, S.; Wu, D. The design of a multifunctional separator regulating the lithium ion flux for advanced lithium-ion batteries. *RSC Adv.* **2019**, *9*, 40084–40091. [[CrossRef](#)]
12. Wang, Z.; Chen, J.; Ye, B.; Pang, P.; Ma, Z.; Chen, H.; Nan, J. A pore-controllable polyamine (PAI) layer-coated polyolefin (PE) separator for pouch lithium-ion batteries with enhanced safety. *J. Solid State Electrochem.* **2020**, *24*, 843–853. [[CrossRef](#)]
13. Lee, Y.; Lee, H.; Lee, T.; Ryou, M.H.; Lee, Y.M. Synergistic thermal stabilization of ceramic/co-polyimide coated polypropylene separators for lithium-ion batteries. *J. Power Sources* **2015**, *294*, 537–544. [[CrossRef](#)]
14. Li, W.; Li, X.; Yuan, A.; Xie, X.; Xia, B. Al₂O₃/poly(ethylene terephthalate) composite separator for high-safety lithium-ion batteries. *Lonics* **2016**, *22*, 2143–2149. [[CrossRef](#)]
15. Ding, L.; Yan, N.; Zhang, S.; Xu, R.; Wu, T.; Yang, F.; Cao, Y.; Xiang, M. Low-Cost Mass Manufacturing Technique for the Shutdown-Functionalized Lithium-Ion Battery Separator Based on Al₂O₃ Coating Online Construction during the β -iPP Cavitation Process. *ACS Appl. Mater. Interfaces* **2022**, *14*, 6714–6728. [[CrossRef](#)] [[PubMed](#)]
16. Parikh, D.; Jafta, C.J.; Thapaliya, B.P.; Sharma, J.; Meyer, H.M., III; Silkowski, C.; Li, J. Al₂O₃/TiO₂ coated separators: Roll-to-roll processing and implications for improved battery safety and performance. *J. Power Sources* **2012**, *507*, 230259. [[CrossRef](#)]
17. Shekarian, E.; Nasr, M.R.J.; Mohammadi, T.; Bakhtiari, O.; Javanbakht, M. Enhanced Wettability and Electrolyte Uptake of Coated Commercial Polypropylene Separators with Inorganic Nanopowders for Application in Lithium-ion Battery. *J. Nanostruct.* **2019**, *9*, 736–750. [[CrossRef](#)]
18. Zheng, H.; Wang, Z.; Shi, L.; Zhao, Y.; Yuan, S. Enhanced thermal stability and lithium ion conductivity of polyethylene separator by coating colloidal SiO₂ nanoparticles with porous shell. *J. Colloid Interface Sci.* **2019**, *554*, 29–38. [[CrossRef](#)]
19. Xu, Q.; Kong, Q.; Liu, Z.; Wang, X.; Liu, R.; Zhang, J.; Yue, L.; Duan, Y.; Cui, G. Cellulose/Polysulfonamide Composite Membrane as a High Performance Lithium-Ion Battery Separator. *ACS Sustain. Chem. Eng.* **2014**, *2*, 194–199. [[CrossRef](#)]
20. Pan, R.; Xu, X.; Sun, R.; Wang, Z.; Lindh, J.; Edstrom, K.; Stromme, M.; Nyholm, L. Nanocellulose Modified Polyethylene Separators for Lithium Metal Batteries. *Small* **2018**, *14*, e1704371. [[CrossRef](#)]
21. Sheng, J.; Tong, S.; He, Z.; Yang, R. Recent developments of cellulose materials for lithium-ion battery separators. *Cellulose* **2017**, *24*, 4103–4122. [[CrossRef](#)]
22. Chun, S.J.; Choi, E.S.; Lee, E.H.; Kim, J.H.; Lee, S.Y.; Lee, S.Y. Eco-friendly cellulose nanofiber paper-derived separator membranes featuring tunable nanoporous network channels for lithium-ion batteries. *J. Mater. Chem.* **2012**, *22*, 16618–16626. [[CrossRef](#)]
23. Pan, R.; Wang, Z.; Sun, R.; Lindh, J.; Edstrom, K.; Stromme, M.; Nyholm, L. Polydopamine-based redox-active separators for lithium-ion batteries. *J. Mater.* **2019**, *5*, 204–213. [[CrossRef](#)]
24. Wang, Z.; Pan, R.; Sun, R.; Edstrom, K.; Stromme, M.; Nyholm, L. Nanocellulose Structured Paper-Based Lithium Metal Batteries. *ACS Appl. Energy Mater.* **2018**, *1*, 4341–4350. [[CrossRef](#)]
25. Huang, Q.; Zhao, C. Bacterial cellulose nanofiber membrane for use as lithium-ion battery separator. *IOP Conf. Ser. Earth Environ. Sci.* **2021**, *647*, 012069. [[CrossRef](#)]
26. Kim, J.H.; Gu, M.; Lee, D.H.; Kim, J.H.; Oh, Y.S.; Min, S.H.; Kim, B.S.; Lee, S.Y. Functionalized Nanocellulose-Integrated Heterolayered Nanomats toward Smart Battery Separators. *Nano Lett.* **2016**, *16*, 5533–5541. [[CrossRef](#)]
27. Choi, W.; Kang, Y.; Kim, I.J.; Seong, B.G.; Yu, W.R.; Kim, D.W. Stable Cycling of a 4 V Class Lithium Polymer Battery Enabled by In Situ Cross-Linked Ethylene Oxide/Propylene Oxide Copolymer Electrolytes with Controlled Molecular Structures. *ACS Appl. Mater. Interfaces* **2021**, *13*, 35664–35676. [[CrossRef](#)]
28. Kim, H.; Kim, D.Y.; Suk, J.; Kang, Y.; Lee, J.B.; Kim, H.J.; Kim, D.W. Stable cycling via absolute intercalation in graphite-based lithium-ion battery incorporated by solidified ether-based polymer electrolyte. *Mater. Adv.* **2021**, *2*, 3898–3905. [[CrossRef](#)]
29. Jeon, H.; Yeon, D.; Lee, T.; Park, J.; Ryou, M.H.; Lee, Y.M. A water-based Al₂O₃ ceramic coating for polyethylene-based microporous separator for lithium-ion batteries. *J. Power Sources* **2016**, *315*, 161–168. [[CrossRef](#)]
30. Kennedy, S.; Kim, J.T.; Lee, Y.M.; Rhiri, I.; Ryou, S.Y. Upgrading the Properties of Ceramic-Coated Separator for Lithium Secondary Batteries by Changing the Mixing Order of the Water-Based Ceramic Slurry Components. *Batteries* **2022**, *8*, 64. [[CrossRef](#)]
31. Liu, X.; Wei, S.; Ning, R.; Sun, Z.; Li, X. Preparation and Characteristics of Lithium Battery Separator Based on Cellulose Modification by Water-Soluble Polyimide Impregnated. *IOP Conf. Ser. Earth Environ. Sci.* **2021**, *687*, 012119. [[CrossRef](#)]
32. Gou, J.; Liu, W.; Tang, A. A novel method to prepare a highly porous separator based on nanocellulose with multi-scale pore structures and its application for rechargeable lithium ion batteries. *J. Membr. Sci.* **2021**, *639*, 119750. [[CrossRef](#)]
33. Xu, R.; Sheng, L.; Gong, H.; Kong, Y.; Yang, Y.; Li, M.; Bai, Y.; Song, S.; Liu, G.; Wang, T.; et al. High-Performance Al₂O₃/PAALi Composite Separator Prepared by Water-Based Slurry for High-Power Density Lithium-Based Battery. *Adv. Eng. Mater.* **2020**, *23*, 2001009. [[CrossRef](#)]
34. Yang, C.; Tong, H.; Luo, C.; Yuan, S.; Chen, G.; Yang, Y. Boehmite particle coating modified microporous polyethylene membrane: A promising separator for lithium ion batteries. *J. Power Sources* **2017**, *348*, 80–86. [[CrossRef](#)]

35. Ryu, J.; Han, D.Y.; Hong, D.; Park, S. A polymeric separator membrane with chemoresistance and high Li-ion flux high-energy-density lithium metal batteries. *Energy Storage Mater.* **2022**, *45*, 941–951. [[CrossRef](#)]
36. Li, J.; Wang, Q.; Wang, Z.; Cao, Y.; Zhu, J.; Lou, Y.; Zhao, Y.; Shi, L.; Yuan, S. Evaporation and in-situ gelation induced porous hybrid film without template enhancing the performance of lithium ion battery separator. *J. Colloid Interface Sci.* **2021**, *595*, 142–150. [[CrossRef](#)]
37. Wang, Y.; Yin, C.; Song, Z.; Wang, Q.; Lan, Y.; Luo, J.; Bo, L.; Yue, Z.; Sun, F.; Li, X. Application of PVDF Organic Particles Coating on Polyethylene Separator for Lithium Ion Batteries. *Materials* **2019**, *12*, 3125. [[CrossRef](#)]
38. Thiangtham, S.; Saito, N.; Manuspiya, H. Asymmetric Porous and Highly Hydrophilic Sulfonated Cellulose/Biomembrane Functioning as a Separator in a Lithium-Ion Battery. *ACS Appl. Energy Mater.* **2022**, *5*, 6206–6218. [[CrossRef](#)]
39. Zhang, T.; Qu, H.; Sun, K. Development of polydopamine coated electrospun PAN/PMMA nanofibrous membrane as composite separator for lithium-ion batteries. *Mater. Lett.* **2019**, *245*, 10–13. [[CrossRef](#)]
40. Lei, O.K.; Zhang, Q.; Wu, X.Y.; Wei, X.; Zhang, J.; Wang, K.X.; Chen, J.S. Towards ultra-stable lithium metal batteries: Interfacial ionic flux regulated through LiAl LDH-modified polypropylene separator. *Chem. Eng. J.* **2020**, *395*, 125187. [[CrossRef](#)]
41. Li, D.; Wang, H.; Luo, L.; Zhu, J.; Li, J.; Liu, P.; Yu, Y.; Jiang, M. Electrospun Separator Based on Sulfonated Polyoxadiazole with Outstanding Thermal Stability and Electrochemical Properties for Lithium-Ion Batteries. *ACS Appl. Energy Mater.* **2021**, *4*, 879–887. [[CrossRef](#)]
42. Xu, W.; Wang, J.; Ding, F.; Chen, X.; Nasybulin, E.; Zhang, Y.; Zhang, J.G. Lithium metal anodes for rechargeable batteries. *Energy Environ. Sci.* **2014**, *7*, 513–537. [[CrossRef](#)]
43. Zhang, J.G.; Xu, W.; Xiao, J.; Cao, X.; Liu, J. Lithium Metal Anodes with Nonaqueous Electrolytes. *Chem. Rev.* **2020**, *120*, 13312–13348. [[CrossRef](#)]
44. Sun, F.; He, X.; Jiang, X.; Osenberg, M.; Li, J.; Zhou, D.; Dong, K.; Hilger, A.; Zhu, X.; Gao, R.; et al. Advancing knowledge of electrochemically generated lithium microstructure and performance decay of lithium ion battery by synchrotron X-ray tomography. *Mater. Today* **2019**, *27*, 21–32. [[CrossRef](#)]
45. Sun, F.; Zielke, L.; Markötter, H.; Hilger, A.; Zhou, D.; Moroni, R.; Zengerle, R.; Thiele, S.; Banhart, J.; Manke, I. Morphological Evolution of Electrochemically Plated/Stripped Lithium Microstructures Investigated by Synchrotron X-ray Phase Contrast Tomography. *ACS Nano* **2016**, *10*, 7990–7997. [[CrossRef](#)]
46. Sun, F.; Moroni, R.; Dong, K.; Markötter, H.; Zhou, D.; Hilger, A.; Zielke, L.; Zengerle, R.; Thiele, S.; Banhart, J.; et al. Study of the Mechanisms of Internal Short Circuit in a Li/Li Cell by Synchrotron X-ray Phase Contrast Tomography. *ACS Energy Lett.* **2017**, *2*, 94–104. [[CrossRef](#)]
47. Sun, F.; Osenberg, M.; Dong, K.; Zhou, D.; Hilger, A.; Jafta, C.J.; Risse, S.; Lu, Y.; Markötter, H.; Manke, I. Correlating Morphological Evolution of Li Electrodes with Degrading Electrochemical Performance of Li/LiCoO₂ and Li/S Battery Systems: Investigated by Synchrotron X-ray Phase Contrast Tomography. *ACS Energy Lett.* **2018**, *3*, 356–365. [[CrossRef](#)]
48. Sun, F.; Yang, C.; Manke, I.; Chen, L.; Dong, S. Li-based anode: Is dendrite-free sufficient? *Mater. Today* **2020**, *38*, 7–9. [[CrossRef](#)]
49. Sun, F.; Gao, R.; Zhou, D.; Osenberg, M.; Dong, K.; Kardjilov, N.; Hilger, A.; Markötter, H.; Bieker, P.M.; Liu, X.; et al. Revealing Hidden Facts of Li Anode in Cycled Lithium–Oxygen Batteries through X-ray and Neutron Tomography. *ACS Energy Lett.* **2019**, *4*, 306–316. [[CrossRef](#)]
50. Sun, F.; Zhou, D.; He, X.; Osenberg, M.; Dong, K.; Chen, L.; Mei, S.; Hilger, A.; Markötter, H.; Lu, Y.; et al. Morphological Reversibility of Modified Li-Based Anodes for Next-Generation Batteries. *ACS Energy Lett.* **2020**, *5*, 152–161. [[CrossRef](#)]
51. Huang, Z.; Chen, Y.; Han, Q.; Su, M.; Liu, Y.; Wang, S.; Wang, H. Vapor-induced phase inversion of poly (m-phenylene isophthalamide) modified polyethylene separator for high-performance lithium-ion batteries. *Chem. Eng. J.* **2022**, *429*, 132429. [[CrossRef](#)]
52. Choi, J.; Yang, K.; Bae, H.S.; Phiri, I.; Ahn, H.J.; Won, J.C.; Lee, Y.M.; Kim, Y.H.; Ryou, M.H. Highly Stable Porous Polyimide Sponge as a Separator for Lithium-Metal Secondary Batteries. *Nanomaterials* **2020**, *10*, 1976. [[CrossRef](#)] [[PubMed](#)]
53. Choi, S.; Mugobera, S.; Ko, J.M.; Lee, K.S. Dendrite-suppressing separator with high thermal stability by rod-like ZnO coating for lithium batteries. *Colloids Surf. A Physicochem. Eng. Asp.* **2021**, *631*, 127722. [[CrossRef](#)]
54. Yin, Y.; Zhao, W.; Wang, A.; Yue, H.; Cao, Z.; Shi, Z.; Li, S.; Yang, S. Cation-Selective Dual-Functional Separator as an Effective Polysulfide Barrier and a Li Dendrite Inhibitor for Lithium-Sulfur Batteries. *ACS Appl. Energy Mater.* **2020**, *3*, 11855–11862. [[CrossRef](#)]
55. Han, D.H.; Zhang, M.; Lu, P.X.; Wan, Y.L.; Chen, Q.L.; Niu, H.Y.; Yu, Z.W. A multifunctional separator with Mg(OH)₂ nanoflake coatings for safe lithium-metal batteries. *J. Energy Chem.* **2021**, *52*, 75–83. [[CrossRef](#)]
56. Yang, L.-Y.; Cao, J.-H.; Liang, W.-H.; Wang, Y.-K.; Wu, D.-Y. Effects of the Separator MOF-Al₂O₃ Coating on Battery Rate Performance and Solid–Electrolyte Interphase Formation. *ACS Appl. Mater. Interfaces* **2022**, *14*, 13722. [[CrossRef](#)]
57. Cheng, C.; Liu, H.; Ouyang, C.; Hu, N.; Zha, G.; Hou, H. A high-temperature stable composite polyurethane separator coated Al₂O₃ particles for lithium ion battery. *Compos. Commun.* **2022**, *33*, 101217. [[CrossRef](#)]
58. Liang, T.; Cao, J.-H.; Liang, W.-H.; Li, Q.; He, L.; Wu, D.-Y. Asymmetrically coated LAGP/PP/PVDF–HFP composite separator film and its effect on the improvement of NCM battery performance. *RSC Adv.* **2019**, *9*, 41151. [[CrossRef](#)]
59. Rao, Q.-S.; Liao, S.-Y.; Huang, X.-W.; Li, Y.-Z.; Liu, Y.-D.; Min, Y.-G. Assembly of MXene/PP Separator and Its Enhancement for Ni-Rich LiNi_{0.8}Co_{0.1}Mn_{0.1}O₂ Electrochemical Performance. *Polymers* **2020**, *12*, 2192. [[CrossRef](#)]

60. Li, X.; Liu, K.; Yan, Y.; Yu, J.; Dong, N.; Liu, B.; Tian, G.; Qi, S.; Wu, D. Thermostable and nonflammable polyimide/zirconia compound separator for lithium-ion batteries with superior electrochemical and safe properties. *J. Colloid Interface Sci.* **2022**, *625*, 936. [[CrossRef](#)]
61. Wu, D.; Dong, N.; Wang, R.; Qi, S.; Liu, B.; Wu, D. In situ construction of High-safety and Non-flammable polyimide “Ceramic” Lithium-ion battery separator via SiO₂ Nano-Encapsulation. *Chem. Eng. J.* **2021**, *420*, 129992. [[CrossRef](#)]
62. Han, D.; Wang, X.; Zhou, Y.-N.; Zhang, J.; Liu, Z.; Xiao, Z.; Zhou, J.; Wang, Z.; Zheng, J.; Jia, Z.; et al. A Graphene-Coated Thermal Conductive Separator to Eliminate the Dendrite-Induced Local Hotspots for Stable Lithium Cycling. *Adv. Energy Mater.* **2022**, *12*, 2201190. [[CrossRef](#)]
63. Yu, J.; Dong, N.; Liu, B.; Tian, G.; Qi, S.; Wu, D. A newly-developed heat-resistance polyimide microsphere coating to enhance the thermal stability of commercial polyolefin separators for advanced lithium-ion battery. *Chem. Eng. J.* **2022**, *442*, 136314. [[CrossRef](#)]
64. Sun, S.; Wang, J.; Chen, X.; Ma, Q.; Wang, Y.; Yang, K.; Yao, X.; Yang, Z.; Liu, J.; Xu, H.; et al. Thermally Stable and Dendrite-Resistant Separators toward Highly Robust Lithium Metal Batteries. *Adv. Energy Mater.* **2022**, *12*, 2202206. [[CrossRef](#)]
65. Yao, H.; Yan, L.; Shen, J.; Wang, T.; Chen, P.; Cong, X.; Zhang, S.; Jiang, H.; Zhao, X. Controllably regulating ion transport in lithium metal batteries via pore effect of metal–organic framework-based separators. *Appl. Surf. Sci.* **2022**, *589*, 152885. [[CrossRef](#)]
66. Zou, Z.; Hu, Z.; Pu, H. Lithium-ion battery separators based-on nanolayer co-extrusion prepared polypropylene nanobelts reinforced cellulose. *J. Membr. Sci.* **2023**, *666*, 121120. [[CrossRef](#)]
67. Hu, W.; Fu, W.; Jhulki, S.; Chen, L.; Narla, A.; Sun, Z.; Wang, F.; Magasinski, A.; Yushin, G. Heat-resistant Al₂O₃ nanowire-polyetherimide separator for safer and faster lithium-ion batteries. *J. Mater. Sci. Technol.* **2023**, *142*, 112. [[CrossRef](#)]
68. Baek, M.; Yoo, J.; Kim, Y.; Seo, H.; Lee, S.-M.; Jo, H.; Woo, S.-G.; Kim, J.-H. Surface Modification of Polyethylene Separator for Li-Ion Batteries via Imine Formation. *Int. J. Energy Res.* **2023**, *2023*, 4624762. [[CrossRef](#)]
69. Kim, Y.; Jang, Y.-J.; Seo, H.; Lee, J.-N.; Woo, S.-G.; Kim, J.-H. Poly(ether ether ketone)-Induced Surface Modification of Polyethylene Separators for Li-Ion Batteries. *Energies* **2023**, *16*, 627. [[CrossRef](#)]

Disclaimer/Publisher’s Note: The statements, opinions and data contained in all publications are solely those of the individual author(s) and contributor(s) and not of MDPI and/or the editor(s). MDPI and/or the editor(s) disclaim responsibility for any injury to people or property resulting from any ideas, methods, instructions or products referred to in the content.